Waste Management 130 (2021) 65–73

Contents lists available at ScienceDirect

Waste Management

journal homepage: www.elsevier.com/locate/wasman

Characteristic properties and recyclability of the aluminium fraction of MSWI bottom ash

Mertol Gökelma [a,b,*], Alicia Vallejo-Olivares [b], Gabriella Tranell [b]

[a] Department of Materials Science and Engineering, Izmir Institute of Technology, 35430 Izmir, Turkey
[b] Department of Materials Science and Engineering, Norwegian University of Science and Technology, 7491 Trondheim, Norway

ARTICLE INFO

Article history:
Received 18 February 2021
Revised 9 May 2021
Accepted 11 May 2021

Keywords:
Aluminium
Recycling
Bottom ash
Incineration
MSWI

ABSTRACT

The increasing use of aluminimum in packaging applications results in many different aluminium-based products ending up in consumer mixed-waste bins. This waste is typically incinerated, generating an aluminium-containing bottom ash. The current work investigates the recyclability of the aluminium fraction in the bottom ash from waste incineration plants in the USA, UK and Denmark. Incinerated Al-samples from different size fractions (2–6 mm, 6–12 mm and 12–30 mm) were characterized in terms of inherent oxide thickness, re-melting yield/coagulation and composition. The measured average oxide thickness on Al particles was 68 μm (SD=100), with the metal yield and coagulation efficiency measured to between 76 and 92% and 87–99% respectively. Larger particle size fractions resulted in a higher metal yield due to their higher mass to surface ratio. A simplified model correlating metal yield and particle size was proposed. The aluminium content of the melted material was determined to between 95.6 and 98.5% with main impurities being Fe, Si, Mn, Zn, Mg and Cu, corresponding to major aluminium alloying elements and waste charge components.

1. Introduction

The production of aluminium has increased rapidly over the last decades due to an increasing consumer population and new application areas of this versatile metal. The global aluminium consumption in 2019 was 89.9 million mt (Hydro Annual Report, 2019), of which 26% was used for transport, 24% for construction, 11% for each of the categories electrical goods and machinery, 8% for each of the packaging and foil stock applications and 6% for consumer durables. Packaging products have a relatively short lifetime, and their waste management has been the focus of recent environmental regulations in Europe (Directive (EU) 2018/852), which state that by 2025 at least 50% by weight of the aluminium packaging must be recycled; 60% by 2030.

A part of the used aluminium packaging materials is collected and recycled with the help of deposit-refund systems and/or sorted household curb-side collection. However, in many countries, and particularly those with a low collection rate, household packaging scrap is thrown in the waste bin and end up at incineration facilities or landfills, depending on the regulations of the corresponding country (Hoornweg & Bhada-Tata, 2012). 47.4% of municipal waste was recycled in the European Union in 2018. The highest recycling rate was achieved in Germany with 67.3% while 49.9% was recycled in Denmark, and 44.1% in United Kingdom (Eurostat, 2020). The recycling rate of municipal waste in the USA is approximately 25% (2017) which is lower than the average rate in the EU. Approximately 139.6 MT municipal solid waste was landfilled in the USA, which is over 50% of the total amount (EPA, 2021).

Incinerating household waste is a way to reduce landfilling while generating thermal energy that could be converted to electricity or used for heating. During the predominant type of incineration, the waste is conveyed through an incineration zone, burning its organic content and generating temperatures as high as 1100 °C (Bunge, 2016). Grate-firing technology is the most common incineration method however the fluidized bed is also used in the US (20%) and Europe (5%) (Leckner and Lind, 2020). After incineration, the bottom ash is sorted out for utilisation/recycling into different fractions: minerals (50-70 wt%), glass and ceramics (10-30 wt%), ferrous metals (5-15 wt%) and non-ferrous metals (1-5 wt%) (Šyc et al., 2020). About 16.5 Mt incineration bottom ash (IBA) is generated per year as a result of roughly 84.5 Mt incinerated municipal solid waste in the EU (Blasenbauer et al., 2020).

Up to 2.2% of the overall mass of incineration bottom ash consists of aluminium (Šyc et al., 2018). Recovering the aluminium from the IBA makes economic and environmental sense, since the energy consumption and related greenhouse emissions of

* Corresponding author at: Department of Materials Science and Engineering, Izmir Institute of Technology, 35430 Izmir, Turkey.
E-mail address: mertolgokelma@iyte.edu.tr (M. Gökelma).

https://doi.org/10.1016/j.wasman.2021.05.012
0956-053X/

recycling aluminium via re-melting are considerably lower than that of primary Al production (Rüttinger et al., 2016). However, the recyclable aluminium content is not well established due to the high oxygen affinity of aluminium and subsequent oxidation/metal loss during incineration (Hu et al., 2011). Warrings and Fellner (2018) reported that approximately 11% of the aluminium mass is oxidized during incineration, while Bunge (2016) stated that a third of the mass of used beverage cans (UBCs) is oxidized if they undergo this process. The oxidation of aluminium alloys is a time and temperature dependent phenomenon (Smith et al., 2018b ; Thiele, 1962). The exposure to high temperatures and a heterogenous furnace atmosphere due to variable incinerator charges, causes a wide range of oxidation behaviours, as well as losses due to the formation of aluminium nitride (Bunge, 2016). In addition to temperature and atmosphere, the degree of oxidation may also be affected by different scrap parameters such as thickness, surface area, coatings/contamination and alloy chemical composition. Numerous studies have shown the critical effect of magnesium content (Field et al., 1987 ; Kim et al., 1996 ; Rossel, 1990; Tabereaux and Peterson, 2014), as well as thickness and surface area (Rossel, 1990; Xiao and Reuter, 2002; Xiao et al., 2000) on the recyclability of aluminium.

Since the melting point of pure aluminium is 660 °C (Totten et al., 2018), the scrap melts during incineration and solidify into different shapes and sizes, which are typically sieved into different size fractions and commercialized separately due to their differences in recyclability (Biganzoli et al., 2014; Gökelma et al., 2019; Hu and Bakker,2015). The reason behind such differences might be higher specific oxide content in the smaller pieces. Another factor could be the chemical composition or surface area of the initial scrap that form each fraction. According to Hu and co-workers, the type of scrap determines the bottom ash particle size, e.g. 86% of the UBCs end up in the + 6 mm size fraction (Hu et al., 2011). Therefore, hypothetically a higher % magnesium content could be expected in this fraction, since the alloy 3004, which is high in magnesium, is used generally for the lids which constitutes 25% of the mass of the UBCs (Totten et al., 2018). Household foil on the other hand, which generally has a low recycling yield attributed to its thickness (Hu et al., 2011; Schlesinger, 2017), mostly ends up in the 2–6 mm fraction.

The goal of the current work was to investigate the correlation between particle size, level of oxidation, impurity element content and recyclability of the aluminium fraction from IBA generated in three different countries (USA, UK and Denmark) with the size fractions of 2–6, 6–12, and 12–30 mm.

2. Materials and methods

2.1. Materials

Dry sorted aluminium fractions of bottom ash from MSWI plants were received from a European recycling company. The eight IBA samples (5 kg each) were received from incineration plants in the USA, UK and Denmark. The samples from the USA and UK were received in three size ranges (2–6, 6–12, 12–30 mm) while samples from Denmark were produced in two size ranges (2–12, 12–30 mm).

To ease the comparison with the UK and USA samples, 0.5 kg of the DK size fraction 2–12 mm was sieved with a 6 mm mesh size. This revealed that 2/3 of the mass fell within the size range 2–6 mm and 1/3 within 6–12 mm. However, the remaining original fraction DK 2–12 (4.5 kg) was kept for the experimental study as provided by industry since the manual sorting in the laboratory might not represent the machine sorting used in the industry.

2.2. Aspect ratio and mass analysis of bottom ash

The aluminium pieces in all size ranges can be found in a large variety of shapes. Aspect ratio [A_R = min ferret/max ferret (Merkus, 2010)] is a common method to identify the shape characteristics of an object. Pictures of 50 g (typically 20–150 pieces) of each sample size were taken and processed by using the image analysis software ImageJ (Schneider et al.). The minimum and maximum axis of each sample was measured and the A_R was calculated accordingly. Furthermore, the average mass of the bottom ash samples was calculated by weighing 20 random samples from each group (UK 2–6, 6–12, 23–30, USA 2–6, 6–12, 23–30, DK 2–12-12–30).

2.3. Characterisation of oxide thickness and composition of bottom ash

Three random samples were picked from each of the eight sample groups. The 24 random samples were mounted in epoxy and sectioned into mirrored pieces for oxide layer characterization by the SEM (Zeiss Ultra 55LE FEG-SEM). The oxide layer thicknesses were measured in at least 15 different positions of each sample. EDS was used for approximate analysis of the oxide and metal composition for each piece. The Kruskal-Wallis method (Ostertagová et al., 2014) was used to analyse whether the different size fractions could be considered statistically as identical populations.

2.4. Re-melting setup and procedure

A resistance heating furnace and a ceramic crucible (Al_2O_3-SiO_2) was used for the re-melting experiments. The re-melting was carried out under a salt flux mixture to break the oxide layer, protect against further oxidation and coalesce the aluminium (Besson et al., 2011; Sydykov et al., 2002). 100 g of the salt flux with a composition of 49 wt% NaCl, 49 wt% KCl and 2 wt% CaF_2 was melted in the crucible. After the salt bath reached 800 °C, 50 g of bottom ash sample was added into the bath in four portions of equal mass. Between each charge, the melt was held for 15 min to ensure that the aluminium pieces melted, and that the salt bath again reached 800 °C before adding a new charge. At the end of each experiment, manual stirring was applied for 5 s before the furnace was shut down. The metal and salt were separated by crushing in mortar and washing in water. After the salt was washed out, the metal part was sieved out and separated into two fractions which were coagulated and non-coagulated by measuring the upper size limit of the droplet (usl). The usl of each size fraction was taken as the lowest size of a coagulated droplet and coagulation efficiency (CE) was calculated accordingly.

$CE = \frac{m_{droplets>usl}}{m_{total}} * 100$ (1) where, $m_{droplets\ >\ usl}$ is the weight of particles larger than 6, 12 and 30 mm for the size ranges 2–6, 6–12 and 12–30 mm respectively and m_{total} is the total mass of recovered metal after the re-melting.

In addition, metal yield was calculated after each experiment to assess how much metal can be recovered by re-melting.

Metal Yield $= \frac{m_{total}}{m_{inputmaterial}} * 100$ (2) where, $m_{input\ material}$ is the charged bottom ash scrap for the re-melting.

The same procedure was applied for each sample group and in total 26 re-melting experiments were performed including at least 3 repetitions for each trial. After the re-melting procedure, the solidified samples were cut by a diamond wheel into pieces (1.5–2 g) and the chemical composition of the samples with the closest metal yield to the average value of each fraction were analysed by ICP-MS. The samples were digested with HCl and HNO_3.

3. Results

3.1. Characterization of the bottom ash samples

3.1.1. Physical properties

The results of measurements (25 samples for each fraction) of average weight, axis length and aspect ratio are summarized in Table 1. An increase in the average weight and the axis length was observed with increasing size range as expected. The deviation in aspect ratio and weight between different samples can be explained by the irregular shape of the samples and their behaviour during the sieving process.

3.1.2. Oxide layer thickness

Samples from each size fraction of the materials from USA, UK and Denmark were analysed by SEM. Fig. 1 shows the oxide layer thickness values for each size fraction and country. The graph was plotted by using 437 measurements in 24 random samples. The largest deviation between different samples was observed in the bottom ash from Denmark in which the thickness ranged from < 1 μm up to approximately 2.5 mm. The smallest differences were observed in the samples from the USA. Furthermore, most of the individual samples also showed a heterogeneous oxide thicknesses throughout the surfaces as it can be seen in Fig. 1 by the scattered analysis result per sample.

Table 2 summarises the minimum, maximum and mean thickness values of the oxide layer measured in each of the 24 samples, as well as the sample diameter (maximum axis of the surface analysed by SEM) and the magnesium content of the matrix measured by EDS point analysis.

The mean oxide thicknesses of each sample are shown in Table 2 as a function of measured magnesium content in the matrix. Most of the measurements lay below the 100 μm and the oxide/metal ratio increased with decreasing size fraction. The oxide/metal ratio is the ratio between the mass of the oxide and the mass of the metal. No direct correlation was observed between the mean oxide layer thickness and the magnesium content in the alloy, as elaborated in the discussion. Sample 21, which had a relatively high

Table 1
Characteristics of bottom ash samples for different size fractions and sources.

Country	UK			USA			DK	
Size fraction (mm)	2–6	6–12	12–30	2–6	6–12	12–30	2–12	12–30
Av. weight (g)	0.21	1.25	4.31	0.24	1.07	3.89	0.65	5.04
St. Dev. (g)	0.12	0.66	2.36	0.25	0.61	3.44	0.37	5.10
Aspect ratio	0.533	0.471	0.619	0.488	0.611	0.594	0.635	0.527
St. Dev.	0.31	0.24	0.16	0.27	0.18	0.20	0.19	0.09
Av. axis length (mm)	8	11.5	18.4	9	12.1	19.1	11.8	18.3
St. Dev. (mm)	2.1	2.1	5.2	2.1	2.9	4.1	3.1	6.6

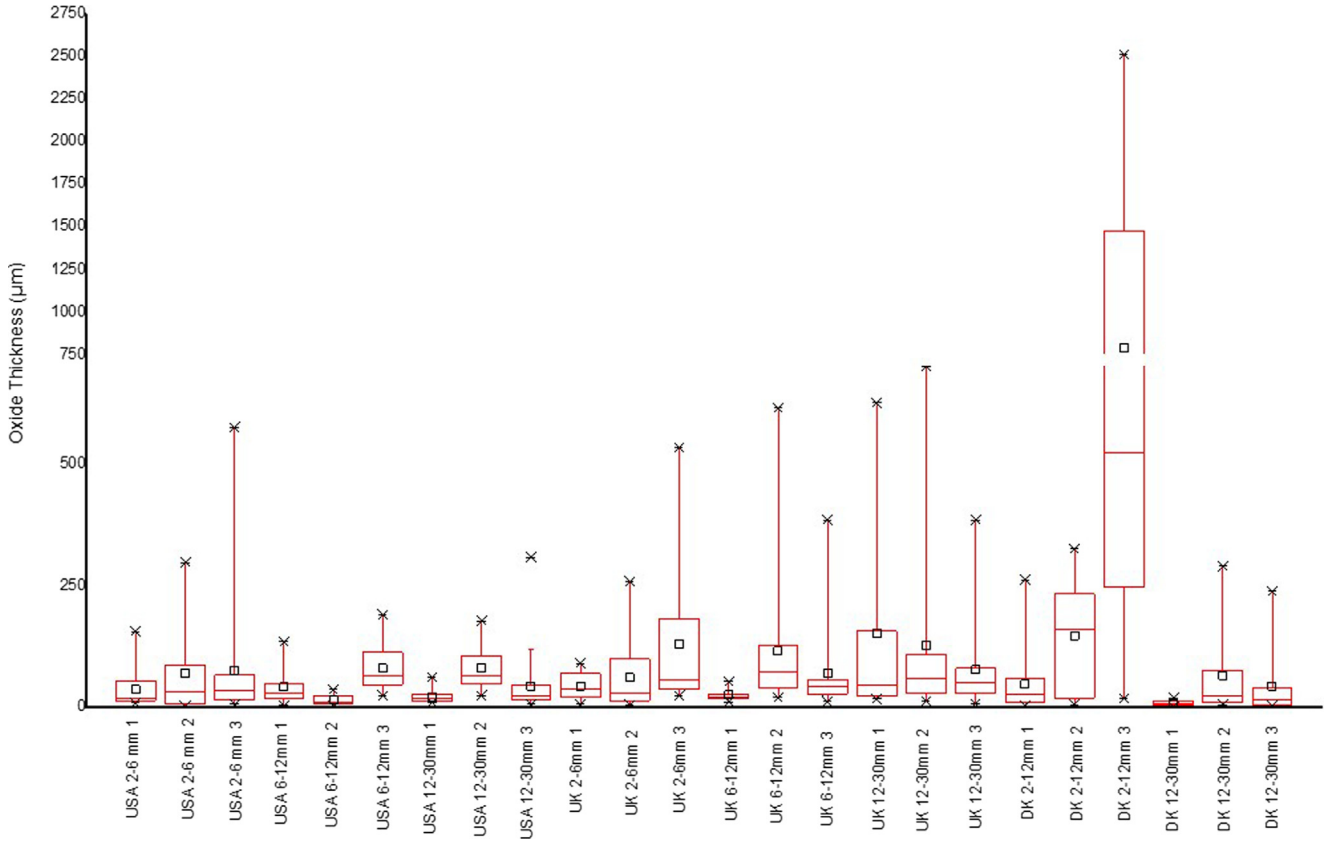

Fig. 1. Oxide thickness measurements of 24 random aluminium IBA samples.

Table 2
Summary of oxide thickness measurements and magnesium content, as measured by EDS in the SEM of each sample.

Sample	Country	Size fraction (mm)	Max axis of the actual particle (mm)	Oxide thickness (μm)			Mg in the alloy (wt%)
				min	max	mean	
1	USA	2–6	6	8.3	155.5	36.2	0.8
2		2–6	7	2.1	297.6	68.8	0.8
3		2–6	7.5	5.9	575.3	74.7	0.9
4		6–12	14.5	3.7	135	41.3	1.8
5		6–12	11	1.4	36.2	13.4	0.9
6		6–12	10.5	23.5	189.7	79.3	0.8
7		12–30	22	8.3	61.2	21.6	2.5
8		12–30	14.5	24	177.4	80.7	1.2
9		12–30	20	6	55.9	42.6	0.8
10	UK	2–6	5	6.1	89.5	46.2	0.8
11		2–6	3	4	258.4	60.5	0.8
12		2–6	3.5	23.6	533.7	129	1.5
13		6–12	11	10.6	52.4	24.4	1.3
14		6–12	11	20	614.4	115.7	0.9
15		6–12	14	12	383.8	69.3	0.9
16		12–30	20.5	16.4	625.3	151	1.2
17		12–30	17	12.3	699.4	127.2	0.9
18		12–30	15.8	6.3	384.4	76.4	1.3
19	DK	2–12	6.6	2.3	261.2	46.5	0.9
20		2–12	6.2	4.5	325.8	146.2	0.9
21		2–12	8.4	17	2512.1	790	1.9
22		12–30	15.7	0.9	18.9	7.4	0.7
23		12–30	13.3	5.1	289.3	65	1
24		12–30	11	2.5	238.5	43.1	1

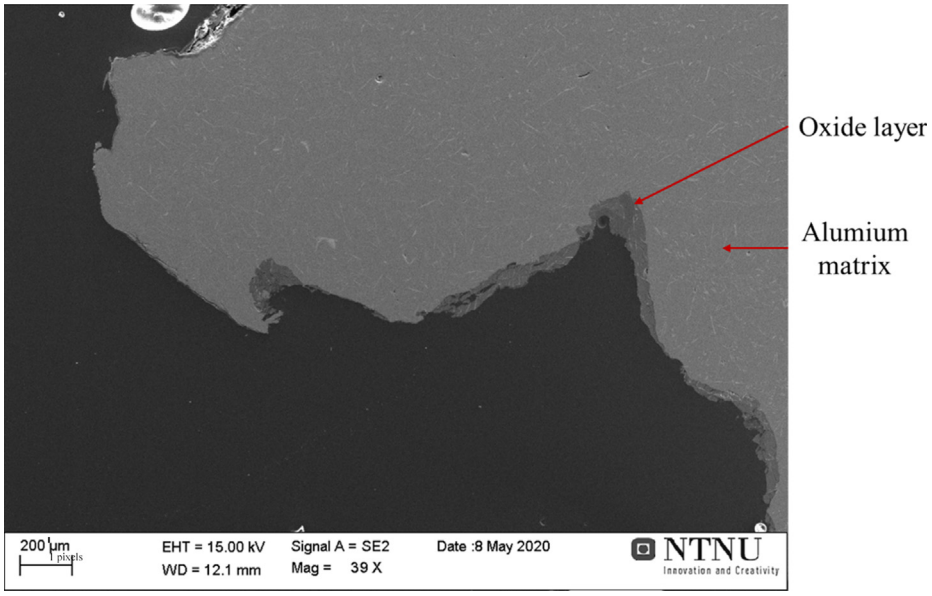

Fig. 2. SEM image of the cross-section of sample 24.

magnesium content, has the largest average oxide thickness value (790 μm) due to a particular heavily oxidized region of the sample. On the other hand, sample 7 with the highest magnesium content had only an average oxide thickness of (22 μm).

Fig. 2 shows sample 24 (DK 12–30) with an average oxidation . The oxide layer (darker part) on the aluminium matrix (lighter part) can be observed clearly in the picture. SEM-EDS analysis was performed to determine the elemental composition of the oxide layer for samples 3, 10, 11, 12 and 23 (from the groups USA 2–6 and UK 2–6) to compare the oxidation behaviour between different samples. Magnesium was found in the range between 0.37 and 0.95 wt% in oxide form and the heavier oxidizied samples generally had higher MgO content in the dross. Exothermic reactions during the incineration may cause an inhomogeneous distribution of oxide growth depending on the position and the surroundings of the samples.

3.2. Re-melting

The metal yield and coagulation efficiency results with mean values and standard deviations (3–5 repetitions for each sample group) are shown in Fig. 3. Metal yield is the most critical parameter to recyclability because it indicates the recyclable metal content in the scrap after subtracting the oxide losses. A clear increase in the metal yield was observed with increasing size range of the samples. The coagulation efficiency of the 2–6 mm samples was, as expected, typically lower than the 6–12 mm and 12–30 mm fractions for the samples from UK and USA. The coagulation

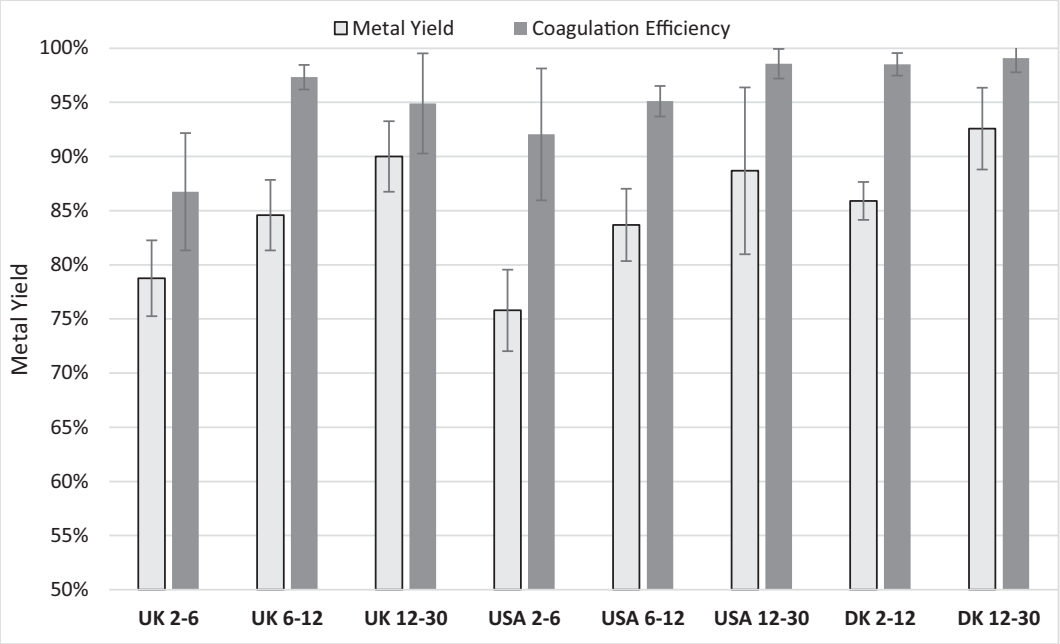

Fig. 3. Metal yield and coagulation efficiency results after re-melting the bottom ash samples under salt flux.

Table 3
Elemental composition (ICP-MS) of remelted aluminium fraction.

Elements (ppm)	UK 2–6 mm	UK 6–12 mm	UK 12–30 mm	USA 2–6 mm	USA 6–12 mm	USA 12–30 mm	DK 2–12 mm	DK 12–30 mm
Cr	133	111	217	198	284	65	210	131
Cu	2240	1630	805	9180	3620	2950	2670	1250
Fe	6080	3900	5680	5860	6380	3780	5020	3590
K	9	5	<0.4	7	33	<0.4	30	<0.8
Mg	357	1020	756	240	654	495	468	1350
Mn	5860	4310	5910	5870	6380	3800	5380	3860
Na	11	8	4	10	33	2	34	4
Ni	71	71	59	277	135	187	74	50
Pb	264	58	169	492	1630	146	418	104
S	2	50	14	15	13	12	18	23
Si	3610	2810	2200	9940	8850	8610	4460	3490
Sn	67	70	9	105	38	36	25	30
Ti	197	232	198	237	219	255	206	130
Y	0.3	0.3	0.5	0.6	0.5	0.8	0.7	0.4
Zn	1880	1010	557	11,100	12,500	1530	3240	2370
Al %	97.9	98.5	98.3	95.6	95.9	97.8	97.8	98.4

efficiency of the two size fractions of DK samples did not deviate significantly from each other.

The aluminium purity was measured by ICP-MS between 95.6 and 98.5 wt%. The elemental composition shows a high variation between the samples and size fractions (Table 3). However, some compositional trends can be observed. As can be expected given typical aluminium alloys, all materials display high concentrations in Cu, Fe, Mg, Mn, Si and Zn. For all three countries, the Cu content is highest in the finest size fraction while the Mg content is highest in the middle fraction. The Si content in all fractions from the US is more than double that of fractions from UK and Denmark. The Ni and Zn contents are also significantly higher in the US material compared to the European materials. Of note is also the seemingly high Pb content in all samples.

4. Discussion

4.1. Physical properties

The shape and weight of aluminium scraps after incineration generally become very irregular. The sorting is done through sieving the aluminium fraction of the bottom ash into different size fractions at the handling/recycling facility. Homogenity of the size fractions depend on the behaviour of particles during the sieving process. The deviation in aspect ratio of the samples in this study was calculated between 0.09 and 0.31. This illustrates that each individual particle does not necessarily fit a given fraction when all three dimensions are taken into account which is a consequence of the sieving process. This heterogene-

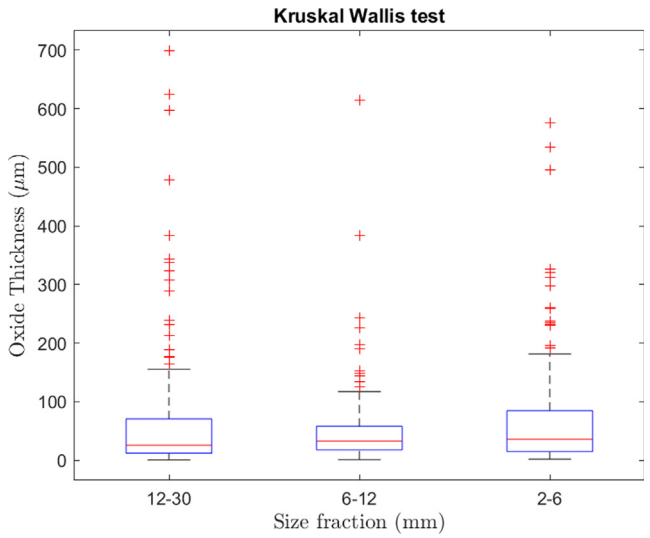

Fig. 4. Kruskal Wallis test graph for size fractions 12–30, 6–12 and 2–6 mm. *The overall average oxide thickness was calculated as 68.12* (SD=100 μm) *for the 413 measurements of 23 samples.*

ity within fractions also causes a variation in the mass of the particles in every size fraction.

4.2. Oxide layer thickness

Although the oxide layer thickness of samples varies, 80% of measurements lay below 100 μm and 90% were below 200 μm of oxide thickness. Fig. 4 presents the Kruskal Wallis test results of the remaining 413 measurements (Chi-square = 2.41, p = 0.229) where the boxes show the interquartile range for each size fraction and the line in the box represents the median of the measurements. As the resultant chi-sq value is below 5.99 and the p value is above 0.05, there is no indication that the sample groups are of a different population. The sample groups can be treated as identical populations with a significance level of 5% and the oxide thickness results can be used to calculate an average. The Kruskal Wallis test showed that the oxide thickness variations are comparable across the different sample groups except for the measurements from the sample 21. Therefore the measurements of sample 21 were not considered for calculating the average.

The magnesium content of the samples did not show a significant correlation to oxide thickness, i.e, the oxide thickness did not increase with increasing magnesium content (Table 2). This indicates that materials containing magnesium do not necessarily over-oxidize during the incineration process. The degree of oxidation can vary depending on the type of waste materials and gases generated around the particle. Protective gases, such as CO_2 form in the process due to the combustion of organic waste products, significantly inhibit the oxidation of magnesium-containing Al alloys (Smith et al., 2018a) . While there was no direct correlation between oxide thickness and magnesium content in the metal of investigated samples, abnormally thick oxide layers were typically associated with a higher magnesium content in the oxide, illustrating the effect of local breakaway oxidation.

4.3. Re-melting

Between 76 and 93% of aluminium was recovered by re-melting of incinerated aluminium fractions for the different size fractions. The results agree with the previous work which focused on the incinerated Norwegian municipal waste where (Gökelma et al., 2019) reported a metal yield of 82 to 93 wt% for the 5–25 mm size fraction. Similar results were reported by other researchers: Biganzoli et al (2014) reported a yield range of 76 to 87 wt% for the size fraction greater than 5 mm aluminium samples from an incineration plant in Italy. Hu and Bakker (2015) stated that the yield of aluminium from household waste composed of different packaging types (beverage cans, containers and foils) ranged between 77 and 93 wt%. Biganzoli and Grosso (2013) studied the operation of two incineration plants and reported that the residence time of the municipal waste between the feeding and the bottom ash extraction was 4–6 h in one plant and 9–10 h in another one. The difference in metal yield between the same input material fraction for different countries may hence be partly caused by plant-specific technology and waste residence time during the incineration.

The increasing metal yield with the increasing size fraction is mainly caused by a decreasing oxide/metal mass ratio. The coagulation efficiency showed an increasing trend with decreasing oxide/metal ratio similar to the metal yield; the salt flux has to dissolve/remove more oxide layer in smaller size fractions because the surface area is larger in smaller size fractions. The larger surface area and oxide/metal ratio may affect the metal yield and the coagulation behaviour negatively. Both coagulation efficiency and metal yield however depend on the recycling method, and thus, an industrial comparison of metal yield should be done for different size fraction materials to verify the laboratory results.

A simplified model, calculating the metal yield as a function of the sample size, is proposed based on the calculated average oxide thickness on the particles. In our model, all samples are assumed to have spherical shape with a real density (ρ_{metal}) of 0.918 g/cm^3 and an oxide density (ρ_{oxide}) of 3.95 g/cm^3 (Gökelma et al., 2019).

$$\text{Theoretical metal yield} = \frac{m_{metal}}{m_{oxide} + m_{metal}}$$

where the mass of the metal was calculated for spherical samples with a diameter varying between 1 and 30 mm and the mass of the oxide was calculated for an 68.12 μm oxide layer covering the corresponding sample surface, using equations (4) and (5).

$$m_{metal} = \rho_{metal} * [4/3 * \pi(r_{sample} - oxidethickness)^3] \quad (4)$$

$$m_{oxide} = \rho_{oxide} * [[4/3 * \pi(r_{sample})^3] - [4/3 * \pi(r_{sample} - oxidethickness)^3]] \quad (5)$$

Fig. 5 shows the theoretical and experimental (UK 2–6: 79%, 6–12: 85%, 12–30: 90%, USA 2–6: 76%, 6–12: 84%, 12–30: 89%, DK 2–12: 86%, 12–30: 93%) results for the metal yield of bottom ash samples. The average axis length values of samples, shown in Table 1, were taken as sample diameter in the model. Although simple, the model shows an acceptable correlation with the experimental test results, which may be used to estimate expected maximum yield in the industrial recycling process.

Most of the theoretical data is slightly above the experimental data which may be due to the metal losses during the re-melting procedure. Similar experimental (re-melting of approximately 3000 pieces) and modelling results indicate that the oxide thickness measurements adequately represent the entire population.

In addition to reasonable metal yield, the alloy composition is also an important factor for recycling. The iron concentration was measured at 3590 to 6380 ppm, without notable variation trends between size fractions and material origin. The silicon concentration was also at the same level throughout the samples analyzed, ranging between 2810 and 9940 ppm. Zinc is found in aluminium beverage can bodies up to 0.25 wt% which may explain the high zinc concentration in the samples. The source of these three elements (Fe, Si and Zn) may be the beverage can bodies

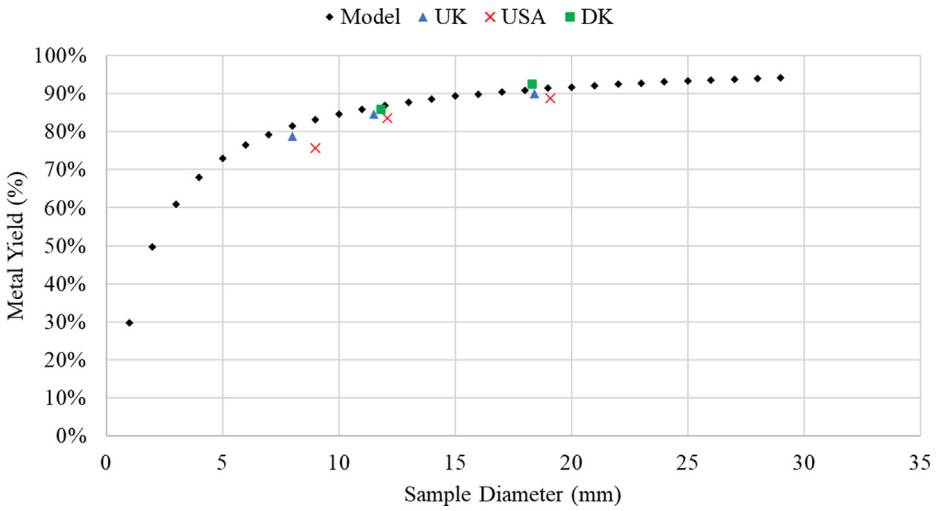

Fig. 5. Comparison of the theoretical and experimental metal yield results.

(Al 3004) and the aluminium screw caps and closures (Al 3105, 8011). The 2–6 and 6–12 mm fractions of the US bottom ash samples contained more than 1% of zinc in the melt. This concentration level is normally not found in packaging alloys and likely originate from Zn evaporation from other Zn-containing materials in the waste charge (such as pennies, zinc-carbon batteries, nuts and bolts).

More statistical data of the aluminium household waste in the different countries is needed in order to explain the compositional differences of the recovered metal. A possible approach is to study the sieving behaviour of the main types of aluminium scrap, and look for correlations between the composition of that type of products and the composition of the remelted metal of the expected size fraction where they would end up. Hu et al. studied the sieving behaviour of aluminium foil containers, beverage cans and thin foil, and found out that 86% of the UBCs end up in the 6–20 mm size fraction (Hu and Bakker,2015). Therefore, hypothetically a higher % magnesium content due to incinerated beverage cans could be expected in the 6–12 mm fraction, since the alloy 5182, which is high in magnesium, is generally used for the lids and constitutes 25% of the mass of the UBCs (Totten et al., 2018). The high magnesium concentration is also reflected in the presented ICP-MS results for the IBA from UK and US. This did not apply to the DK samples, which is explained by the fact that in the DK fraction 2–12 mm, the particles with sizes + 6 mm constituted only 1/3 of the weight. Accordingly, results from Hu et. al showed that most of the thin foils, produced typically from 8011 alloy with a certain iron and silicon concentrations,would end up in the < 2 mm or 2–6 mm fractions. This could explain the slightly higher iron and silicon content found in the ICP-MS results for most of the 2–6 mm fractions.

Manganese is added between 0.5 and 1.5 wt% in 3000 series alloys which are used as sheet products, rigid foil containers and beverage cans (Hu et al., 2011). These alloy materials can be found in almost every size fraction in the bottom ash and subsequently, the manganese concentration was measured to between 3800 and 6380 ppm in all samples. Chromium is present in some of the alloys as a minor element up to 1000 ppm in Al5182 and 500 ppm in Al8011 (Papadopoulou et al., 2020) which are also used in beverage cans and foils respectively (Shi and Shen, 2018). Titanium is typically used as grain refiner and a normal level of addition is approximately 100 ppm. In addition, titanium is found in many wrought alloys as minor element from 100 to 3500 ppm (Sigworth and Kuhn, 2007).

Unpredictable deviations in trace elements is the most important problem for the recycling of complex secondary resources. In the current case, the lead concentrations were considerable with the highest concentration in the 6–12 mm size fraction of the USA sample measuring 1630 ppm. Lead is not commonly alloyed in aluminum however, aluminium alloy 2011 containing up to 0.6 wt% lead is used for making fasteners, fittings, nuts, bolts etc. due to its excellent machinability. Through EU regulations, the permissible level of Pb concentration as trace element in Al alloys has been set at 0.1 wt% (allowing exceptions to the regulation for contents up to 0.4 wt% if the Pb is used as an alloying element) (EC Directive 2015/863/EU) and similar limitations have been set in other countries too. The limitations in the USA market is 0.5 wt% lead in aluminium alloys (Senel, 2019). This may be the reason for higher lead concentrations detected in USA bottom ash samples. Given the legislative limitations, investigations into production of lead free aluminium alloys have been conducted in different research groups (Koch and Antrekowitsch,2011 ;Timelli and Bonollo,2011). Consequently, it is expected that the lead content in bottom ash originating from Al alloys will continuously decrease in the future. As lead has a low melting point and high vapor pressure at elevated temperatures, non-aluminium origins for the measured lead content in the bottom ash is also a possiblity.

The main copper sources in the bottom ash may be the Al5052 and Al8011, used for easy-open lids and foils, which contain copper up to 1000 ppm, the Al2011 and Al3004 containing up to 6 and 0.25 wt% copper respectively. A higher copper concentration was detected in smaller sizes in samples from each country. The copper concentration in the 2–6 mm fraction may be due to the small sized nuts, bolts and fasteners and in the 6–12 mm fraction due to the used beverage cans.

5. Conclusions

Aluminium bottom ash samples from MSWI of different size fraction and country of origin were investigated for characteristic properties and recyclability. The following conclusions were drawn from the investigation:

- The thickness of oxides on the surface of the aluminium samples after incineration can vary from < 1 to several thousand μm depending on the incineration dynamics and the alloy composition of the sample. The thickness measured after incinera-

tion was 68 μm in average over the entire population of samples investigated and oxide thickness has no direct correlation with the size of the particle or country of origin.
- The re-melting metal yield increases with the increasing particle size due to the decreasing oxide/metal ratio. The yield was calculated to between 75.8 and 92.6% with a standard deviation of 3.8%. The USA 2–6 mm samples showed the lowest yield and the DK 12–30 mm resulted in the highest metal yield after re-melting. A simplified model correlating particle size and re-melting yield was developed for spherical samples with a diameter varying between 1 and 30 mm and an 68.12 μm oxide layer covering the sample surface.
- Although magnesium is an important influencing factor for oxidation, the oxide thickness of samples with high magnesium content did not deviate significantly from other samples, which may be due to protective gases, such as CO_2, during the combustion of organic materials surrounding the metal scrap.
- The remelted aluminium materials from all three countries (USA, UK, DK) and size fractions displayed significant contents of Fe, Si, Cu, Mn, Mg and Zn in accordance with typical Al alloy specifications for packaging materials. Materials originating from USA typically showed the highest average concentrations of alloying and trace elements.

The results of the current study may aid in a better understanding of achievable recyclability of incinerated aluminium in terms of metal yield and composition. This is important in e.g the development of improved MFA/LCA models of the aluminium life cycle as well as for operators of aluminium recycling plants.

Declaration of Competing Interest

The authors declare that they have no known competing financial interests or personal relationships that could have appeared to influence the work reported in this paper.

Acknowledgement

The authors wish to thank staff at Blue Phoenix Group for supplying bottom ash samples. Funding was partially provided by the Norwegian Centre for Research-Based Innovation (SFI Metal Production, NFR Project Number 237738.

References

Besson, S.; Pichat, A.; Xolin, E.; Chartrand, P.; Friedrich, B. Improving coalescence in Al-Recycling by salt optimization. In Proceedings of the European Metallurgical Conference, Dusseldorf, Germany, 26–29 June 2011; pp. 1–16. Available online: http://www.metallurgie.rwth-aachen.de/new/images/pages/publikationen/besson_emc2011_id_8928.pdf

Biganzoli, L., Grosso, M., 2013. Aluminium recovery from waste incineration bottom ash, andits oxidation level. Waste Manage. Res. 31 (9), 954–959. https://doi.org/10.1177/0734242x13493956.

Biganzoli, L., Grosso, M., Forte, F., 2014. Aluminium Mass Balance in Waste Incineration and Recovery Potential From the Bottom Ash: A Case Study. Waste Biomass Valorization 5 (1), 139–145. https://doi.org/10.1007/s12649-013-9208-0.

Blasenbauer, D., Huber, F., Lederer, J., Quina, M.J., Blanc-Biscarat, D., Bogush, A., Bontempi, E., Blondeau, J., Chimenos, J.M., Dahlbo, H., Fagerqvist, J., Giro-Paloma, J., Hjelmar, O., Hyks, J., Keaney, J., Lupsea-Toader, M., O'Caollai, C.J., Orupõld, K., Pająk, T., Simon, F.-G., Svecova, L., Šyc, M., Ulvang, R., Vaajasaari, K., Van Caneghem, J.o., van Zomeren, A., Vasarevičius, S., Wégner, K., Fellner, J., 2020. Legal situation and current practice of waste incineration bottom ash utilisation in Europe. Waste Manage. 102, 868–883. https://doi.org/10.1016/j.wasman.2019.11.031.

Bunge, R. (2016). Recovery of metals from waste incinerator bottom ash. https://vbsa.ch/wp-content/uploads/2016/07/Studie-Bunge-Internetversion.pdf

Directive (EU) 2018/852 of the European Parliament and of the Council of 30 May 2018 amending Directive 94/62 / EC on packaging and packaging waste (Text with EEA relevance). (2018). EUR-Lex. https://eur-lex.europa.eu/eli/dir/2018/852/oj

Field, D.J., Scamans, G.M., Butler, E.P., 1987. The high temperature oxidation of Al-4.2 wt pct Mg alloy. Metall. Trans. A 18 (4), 463–472. https://doi.org/10.1007/bf02648807.

Gökelma, M., Meling, I., Soylu, E., Kvithyld, A., Tranell, G., 2019. A Method for Assessment of Recyclability of Aluminum from Incinerated Household Waste. Light Metals 2019, 1359–1365. https://doi.org/10.1007/978-3-030-05864-7_168.

Hoornweg, D., & Bhada-Tata, P. (2012). WHAT A WASTE A Global Review of Solid Waste Management. Urban development series;knowledge papers. http://documents1.worldbank.org/curated/en/302341468126264791/pdf/68135-REVISED-What-a-Waste-2012-Final-updated.pdf

Hu, Y., Bakker, M.C.M., 2015. Recovery of Aluminum Residue from Incineration of Cans in Municipal Solid Waste. J. Residuals Sci. Technol. 12 (3), 157–163 https://doi.org/10.12783/issn.1544-8053/12/3/6.

Hu, Y., Bakker, M.C.M., de Heij, P.G., 2011. Recovery and distribution of incinerated aluminum packaging waste. Waste Manage. 31 (12), 2422–2430. https://doi.org/10.1016/j.wasman.2011.07.021.

Hydro annual report. (2019). https://www.hydro.com/Document/Index?name=Annual%20report%202019%20web.pdf&id=506433

Kim, D.H., Yoon, E.P., Kim, J.S., 1996. Oxidation of an aluminum-0.4 wt% magnesium alloy. J. Mater. Sci. Lett. 15 (16), 1429–1431. https://doi.org/10.1007/bf00275297.

Koch, S., Antrekowitsch, H., 2011. Alloying Behaviour of Cu, Mg and Mn in Lead-free Al-Cu Based Alloys Intended for Free MachiningAuswirkungen der Legierungselemente Cu, Mg und Mn in bleifreien Al-Cu-Automatenlegierungen. BHM Berg- Huettenmaenn. Monatsh. 156 (1), 22–27. https://doi.org/10.1007/s00501-011-0621-z.

Leckner, B., Lind, F., 2020. Combustion of municipal solid waste in fluidized bed or on grate – A comparison. Waste Manage. 109 (2020), 94–108.

Merkus, H.G., 2010. Particle Size Measurements: Fundamentals, Practice, Quality (Particle Technology Series, 17) (Softcover reprint of hardcover. Springer.

Ostertagová, E., Ostertag, O., Kováč, J., 2014. Methodology and Application of the Kruskal-Wallis Test. Applied Mechanics and Materials 611, 115–120. https://doi.org/10.4028/www.scientific.net/amm.611.115.

Papadopoulou, S., Kontopoulou, A., Gavalas, E., Papaefthymiou, S., 2020. The Effects of Reduction and Thermal Treatment on the Recrystallization and Crystallographic Texture Evolution of 5182 Aluminum Alloy. Metals. 10 (10), 1380. https://doi.org/10.3390/met10101380.

Recycling rate of municipal waste. (2020). Eurostat. https://ec.europa.eu/eurostat/databrowser/view/sdg_11_60/default/table

Rossel H. (1990) Fundamental investigations about metal loss during re-melting of extrusion and rolling fabrication scrap. Light Metals 1990, ed. C.M. Bickert, TMS, 721-729, 5. SECAT Press Release.

Rüttinger,L.,Treimer,R.,Tiess,G.,&Griestop,L.(2016).Umwelt-undSozialauswirkungenderBauxitgewinnungundAluminiumherstellunginPará,Brasilien.adelphi.https://www.umweltbundesamt.de/sites/default/files/medien/378/dokumente/umsoress_fallstudie_bauxit_brasilien_finale_version.pdf

Schlesinger, M.E., 2017. Aluminum Recycling. CRC Press.

Senel E., What you need to know about lead-free aluminium alloys. (2019, September 26). Shapes by Hydro. https://www.shapesbyhydro.com/en/material-science/what-you-need-to-know-about-lead-free-aluminium-alloys/

Sigworth, G.K., Kuhn, T.A., 2007. Grain Refinement of Aluminum Casting Alloys. Inter Metalcast 1 (1), 31–40. https://doi.org/10.1007/BF03355416.

Shi, C., Shen, K., 2018. Twin-roll casting 8011 aluminium alloy strips under ultrasonic energy field. International Journal of Lightweight Materials and Manufacture 1 (2), 108–114. https://doi.org/10.1016/j.ijlmm.2018.06.001.

Smith, N., Gleeson, B., Saidi, W.A., Kvithyld, A., Tranell, G., 2018a. Mechanism behind the Inhibiting Effect of CO2 on the Oxidation of Al–Mg Alloys. Ind. Eng. Chem. Res. 58 (3), 1434–1442. https://doi.org/10.1021/acs.iecr.8b04691.

Smith, N., Kvithyld, A., Tranell, G., 2018b. The Mechanism Behind the Oxidation Protection of High Mg Al Alloys with Beryllium. Metallurgical and Materials Transactions B 49 (5), 2846–2857. https://doi.org/10.1007/s11663-018-1340-6.

Šyc, M., Krausová, A., Kameníková, P., Šomplák, R., Pavlas, M., Zach, B., Pohořelý, M., Svoboda, K., Punčochář, M., 2018. Material analysis of Bottom ash from waste-to-energy plants. Waste Manage. 73, 360–366. https://doi.org/10.1016/j.wasman.2017.10.045.

Šyc, M., Simon, F.G., Hykš, J., Braga, R., Biganzoli, L., Costa, G., Funari, V., Grosso, M., 2020. Metal recovery from incineration bottom ash: State-of-the-art and recent developments. J. Hazard. Mater. 393, 122433. https://doi.org/10.1016/j.jhazmat.2020.122433.

Sydykov, A., Friedrich, B., Arnold, A. (2002) Impact of parameter changes on the aluminium recovery in a rotary kiln, in: Schneider, W. A. (ed.), Proceedings of the technical sessions presented by the TMS Aluminium, Light Metals 2002, 131st TMS Annual Meeting, Warrendale, Pennsylvania, USA, pp 1045–1052.

Tabereaux, A.T., Peterson, R.D., 2014. Treatise on Process Metallurgy. Elsevier, 839–917. https://doi.org/10.1016/B978-0-08-096988-6.00023-7.

Thiele, W. (1962). Die Oxydation von Aluminium- und Aluminiumlegierungs-Schmelzen. Erscheinungsort nicht ermittelbar.

Timelli, G., Bonollo, F., 2011. Influence of tin and bismuth on machinability of lead free 6000 series aluminium alloys. Mater. Sci. Technol. 27 (1), 291–299. https://doi.org/10.1179/026708309x12595712305799.

Warrings, R., Fellner, J., 2018. Current status of circularity for aluminum from household waste in Austria. Waste Manage. 76, 217–224. https://doi.org/10.1016/j.wasman.2018.02.034.

Xiao, Y., Reuter, M.A., 2002. Recycling of distributed aluminium turning scrap. Miner. Eng. 15 (11), 963–970. https://doi.org/10.1016/s0892-6875(02)00137-1.

Totten, G.E., Tiryakioğlu, M., & Kessler, O. (Eds.). (2018). Encyclopedia of Aluminum and Its Alloys (1st ed.). CRC Press. https://doi.org/10.1201/9781351045636

Xiao, Y., Reuter, M., Vonk, P., Voncken, J., Orbon, H., Probst, Th.,Boin, U.,(2000). Experimental study on aluminium scrap recycling.In: Stewart Jr., D.L., Daley, J. C., Stephens, R.L., (Eds.), Proceed-ings of the Fourth International Symposium on Recycling of Metals and Engineered Materials, 22–25 October, USA, pp. 1075–1087

National Overview: Facts and Figures on Materials, Wastes and Recycling. (2021). United States Environmental Protection Agency (EPA). https://www.epa.gov/facts-and-figures-about-materials-waste-and-recycling/national-overview-facts-and-figures-materials